ACADEMIC PRESS

Available online at www.sciencedirect.com

SCIENCE DIRECT®

Journal of Sound and Vibration 264 (2003) 523–544

JOURNAL OF SOUND AND VIBRATION

www.elsevier.com/locate/jsvi

Multi-mode sound transmission in ducts with flow

P. Joseph[a,*], C.L. Morfey[a], C.R. Lowis[b]

[a] *Institute of Sound and Vibration Research, University of Southampton, Highfield, Southampton SO17 1BJ, UK*
[b] *DLR-Abteilung Turbulenzforschung, Mueller-Breslau-Str. 8, 10623 Berlin, Germany*

Received 27 February 2002; accepted 24 June 2002

Abstract

Exhaust mufflers, large exhaust stacks, and turbofan engines are common examples of ducted noise. The most useful measure of the sound produced by these noise sources is the sound power transmitted along the duct. When airflow is present, sound power flow can no longer be uniquely determined from the usual measurements of acoustic pressure and particle velocity.

One approach to sound power determination from in-duct pressure measurement, and the one discussed in this paper, is to predict the relationship between the sound power and pressure based upon an assumed mode amplitude distribution. This paper investigates the relationship between acoustic pressure and power for a family of idealized source distributions of arbitrary temporal and spatial order. Incoherent monopole and dipole sources uniformly distributed over a duct cross-section can be obtained as special cases. This paper covers the sensitivity of the pressure–power relationship to source multipole order, frequency and, in particular, flow speed. It is shown that the introduction of flow in a hard-walled duct can have a substantial effect on the behavior of the pressure–power relationship for certain source distributions. Preliminary experimental results in a no-flow facility are presented in order to verify some of the main results.

1. Introduction

Exhaust mufflers, large exhaust stacks, and turbofan engines are common examples of ducted noise. The most useful measure of the sound produced by these noise sources is the sound power transmitted along the duct. Unlike acoustic pressure and other field variables, sound power is a conserved quantity that provides a single index of the source strength. Its measurement, however, is difficult and must usually be inferred from a number of acoustic pressure measurements made, either inside the duct, or in the radiated far field. A fundamental difficulty with making power

*Corresponding author. Tel.: +44-23-8059-2291; fax: +44-23-8059-3190.
E-mail address: pfj@isvr.soton.ac.uk (P. Joseph).

0022-460X/03/$ - see front matter © 2002 Published by Elsevier Science Ltd.
doi:10.1016/S0022-460X(02)01205-1

measurements from in-duct pressure measurements is the presence of airflow. The conventional method of determining sound power from measurements of acoustic intensity is no longer possible when a mean flow is present. Munroe and Ingard [1] show that the usual approach of deducing acoustic particle velocity from the pressure gradient is no longer valid when the direction of flow and sound propagation differs. Under these conditions they show that the relationship between these quantities is non-unique.

Determination of sound power from measurements of acoustic pressure is possible in these situations when there is a priori knowledge of either the source distribution or, equivalently, the mode amplitude distribution. In this case the power–pressure relationship may be determined theoretically, and may then be applied to the pressure measurements to deduce the sound power transmitted along the duct. Unfortunately, the source distribution is rarely known in sufficient detail for this relationship to be applied, and the number of modes may be too large for the amplitudes of individual modes to be measured with sufficient accuracy. An alternative approach, and the one explored in this paper, is to relate the sound power to the measured pressure by assuming an idealized mode amplitude or source distribution. This paper investigates the relationship between pressure and power for a number of idealized source distributions. Of particular interest here is the sensitivity of this relationship to the assumed source distribution and, in particular, the effect of flow speed. For simplicity, the analysis will be restricted to hard walled infinite ducts. The analysis will exclude:

- Reflections from the open end.
- Departure from plug-flow propagation due to shear profile, including the duct wall boundary layer.
- Cut-off modes.
- Measurement noise due to, for example, turbulence.

The effect of these factors on sound power measurement in flow-ducts is discussed extensively in a recent paper by Neise and Arnold [2].

2. Modal transmission

The infinite duct under investigation is presented in Fig. 1.

The in-duct sound field can be expressed as the sum of modal components $p = \sum_{m=-\infty}^{\infty} \sum_{n=0}^{\infty} p_{mn}$, where (m,n) are the usual circumferential and radial mode indices. The

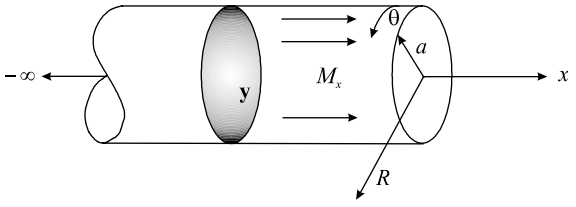

Fig. 1. Semi-infinite, hard walled unflanged circular duct with associated co-ordinate system and continuous source distribution represented by the shaded region.

homogeneous wave equation for sound in a uniform flow is

$$\left(\frac{1}{c^2}\frac{\bar{D}^2}{Dt^2} - \nabla^2\right)p = 0, \tag{1}$$

where $\bar{D}/Dt = \partial/\partial t + cM_x(\partial/\partial x)$ is the convected derivative operator associated with the mean flow velocity $(cM_x,0,0)$ in the $(\mathbf{y},x)$ system and c is the sound speed in the uniform medium. Above its cut-off frequency, at a single frequency ω, a single incident mode of amplitude a_{mn} is described by

$$p_{mn}(\mathbf{y}, x) = \mathrm{e}^{-\mathrm{i}\omega t} a_{mn} \Psi_{mn}(\mathbf{y}) \mathrm{e}^{\mathrm{i}k_{xmn}x}. \tag{2}$$

Substituting Eq. (2) in Eq. (1) gives

$$k_{xmn} = \left(\frac{\alpha_{mn} - M_x}{1 - M_x^2}\right)\frac{\omega}{c}, \tag{3a}$$

$$\alpha_{mn} = \sqrt{1 - (\kappa_{mn}/k)^2(1 - M_x^2)}, \tag{3b}$$

where κ_{mn} are a set of eigenvalues that are characteristic of the duct cross-section such that the corresponding mode shape functions Ψ_{mn}, defined by $\left(\nabla_\perp^2 + \kappa_{mn}^2\right)\Psi_{mn}(\mathbf{y}) = 0$, also satisfy the duct-wall boundary conditions. The sign convention adopted here is such that $M_x > 0$ represents sound propagation in the direction of the flow (duct exhaust) while $M_x < 0$ represents propagating waves in the opposite direction to the flow (duct inlet). The parameter α, which we shall call the cut-on ratio, takes values between $\alpha = 0$ at the modal cut-off frequency $\omega = \omega_{mn} = \kappa_{mn}c(1 - M_x^2)^{1/2}$, and $\alpha = 1$ as $\omega/\omega_{mn} \to \infty$, corresponding to modes well above cut-on.

3. Ratio of sound power to mean square pressure average over a duct cross-section

In this paper, we are concerned with the behavior of the non-dimensional quantity β_S defined by Eq. (4) below. Given β_S, the total transmitted sound power $\bar{W}$ may be deduced from measurements of the mean squared pressure averaged over a duct cross-section, $\langle \overline{p^2} \rangle_S = \frac{1}{2}S^{-1}\int_S pp^* \mathrm{d}S$. The definition of β_S is

$$\bar{W} = \beta_S \frac{S\left\langle \overline{p^2} \right\rangle_S}{\rho c}, \tag{4}$$

where ρ is the mean density. We shall adopt the generalized definition of sound power flow in a uniform axial mean flow given by [3]

$$\bar{W} = \tfrac{1}{2}\int_S \left[\rho c M_x u_x u_x^* + M_x pp^*/\rho c + \tfrac{1}{2}\left(1 + M_x^2\right)\left(pu_x^* + p^* u_x\right)\right]\mathrm{d}S, \tag{5}$$

where u_x denotes axial particle velocity. The time averaged (mean) squared pressure at a position $(\mathbf{y},x)$ in the duct in a narrow frequency band may be written as

$$\overline{p^2}(\mathbf{y},x)=\tfrac{1}{2}\mathrm{E}\left\{\left|\sum_{m,n}a_{mn}\Psi_{mn}(r,\theta)\mathrm{e}^{\mathrm{i}k_{xmn}x}\right|^2\right\},\tag{6}$$

where E{} denotes the expectation. For incoherent excitation we treat the mode amplitudes as uncorrelated random variables so that $\mathrm{E}\{a_{mn}a^*_{m'n'}\}=0$ for $[m,n]\neq[m',n']$, and the summation is restricted to cut-on modes for which $0\leqslant\alpha\leqslant1$ [3], which in Eq. (6) leads to

$$\overline{p^2}(r)=\tfrac{1}{2}\mathrm{E}\{|a_{mn}|^2\}\ \Psi^2_{mn}(r,\theta).\tag{7}$$

This situation is appropriate to many random broadband excitation mechanisms such as unsteady combustion and the turbulence–airfoil interaction responsible for broadband noise generation in turbofan engines. Averaging Eq. (6) in this way removes the dependence on x and θ, suggesting that, for circular ducts for example, the mean squared pressure in the duct is axisymmetric. Note that the presence of reflections at the open end (which are neglected in this investigation) will introduce some axial pressure variation, as observed in, for example, the experimental results presented in Section 8.

The mean squared pressure is now averaged over a duct cross-section S. On making use of the normalization property $S^{-1}\int_S\Psi^2_{mn}(\mathbf{y})\mathrm{d}S=1$, Eq. (7) becomes

$$\left\langle\overline{p^2}\right\rangle_S=\frac{1}{S}\int_S\overline{p^2}\ (\mathbf{y},x)\mathrm{d}S=\tfrac{1}{2}\sum_{m,n}\mathrm{E}\{|a_{mn}|^2\}.\tag{8}$$

This result could have been derived using the orthogonality property of the mode shape functions. Eq. (8) is therefore completely general and is valid even for correlated mode amplitudes. The reason for introducing the assumption of uncorrelated mode amplitudes here is that it will be shown to be a useful approximation when the relationship between sound power and the mean square pressure at the duct wall is investigated in Section 7.

The modal solution of Eqs. (2) and (3), together with the axial particle velocity obtained from the linearized momentum equation, substituted in Eq. (5), leads to the following generalized definition of the time-averaged acoustic sound power carried by a single mode above cut-off in an axial uniform mean flow [3]

$$\bar{W}=\sum_{m,n}\bar{W}_{mn},\quad \bar{W}_{mn}=\frac{S|a_{mn}|^2\alpha_{mn}}{2\rho c}\frac{\left(1-M_x^2\right)^2}{(1-\alpha_{mn}M_x)^2},\tag{9}$$

where S is the duct cross-sectional area and the expectation has been dropped for brevity. Comparison between Eqs. (3a) and (9) makes explicit that the signs of α relate to the direction of energy transmission and not the direction of phase velocities. Eqs. (8) and (9) in Eq. (4) give the following general expression for β_S as

$$\beta_S=\left(1-M_x^2\right)^2\frac{\sum_{m,n}\left[|a_{mn}|^2\alpha_{mn}/(1-\alpha_{mn}M_x)^2\right]}{\sum_{m,n}|a_{mn}|^2}.\tag{10}$$

4. Source models

4.1. Uncorrelated sources of arbitrary spatial and temporal order uniformly distributed over a duct cross-section

In this section, we derive the relationship between the mode amplitudes excited in an infinite hard-walled duct containing an axial mean flow and the cut-on ratio α, for incoherent sources of arbitrary spatial and temporal order uniformly distributed over a duct cross-section. The inhomogeneous wave equation for sound in a uniform flow is

$$\left(\frac{1}{c^2}\frac{\bar{D}^2}{Dt^2} - \nabla^2\right)p = q. \tag{11}$$

Common forms of q are

$$\begin{aligned} q &= \rho\Gamma \quad (\Gamma = \text{volume acceleration source distribution}),\\ q &= \rho\frac{\bar{D}Q}{Dt} \quad (Q = \text{volume velocity distribution}),\\ q &= \rho\frac{\bar{D}^2\sigma}{Dt^2} \quad (\sigma = \text{volume displacement distribution}),\\ q &= \nabla\cdot\mathbf{F} \quad (\mathbf{F} = \text{applied force distribution}). \end{aligned} \tag{12}$$

A generalization of these possibilities is

$$q = \left(\frac{\bar{D}}{Dt}\right)^{\nu}\frac{(-\partial)^{\mu}}{\partial x_i\partial x_j\ldots}q_{ij\ldots}, \tag{13}$$

which represents a source distribution of temporal order ν and spatial order μ. In what follows the source distribution is limited to axial components[1] of q_{ij}. In this case

$$q = \left(\frac{\bar{D}}{Dt}\right)^{\nu}\left(\frac{-\partial}{\partial x}\right)^{\mu}q_{xx\ldots}. \tag{14}$$

Consider a single mode excited in a semi-infinite duct by a source distribution confined to a single-axial location. Under these circumstances Morfey [3] shows that for a single mode the spatial differentials in Eq. (13) are equivalent to

$$\left(\frac{-\partial}{\partial x}\right)^{\mu} \to (-\mathrm{i}k_{xmn})^{\mu}. \tag{15}$$

Similarly, the temporal differential in Eq. (13) may be replaced by

$$\left(\frac{\bar{D}}{Dt}\right)^{\nu} \to \left[-\mathrm{i}\omega + U\frac{\partial}{\partial x}\right]^{\nu} = \left[-\mathrm{i}\omega\left(\frac{1-\alpha M_x}{1-M_x^2}\right)\right]^{\nu}. \tag{16}$$

Combining Eqs. (13)–(16) and following the approach described in, for example, Ref. [4] leads to a general expression for the mode amplitude $|a_{mn}^{(\mu,\nu)}|^2$ excited in a semi-infinite duct by an incoherent source distribution of spatial order μ and temporal order ν, uniformly distributed over a duct

[1] Non-axial components are equivalent to sources of lower order, in the modal formulation.

cross-section:

$$\left|a_{mn}^{(\mu,v)}\right|^2 \propto \frac{1}{\alpha_{mn}^2}\left(\frac{M_x-\alpha_{mn}}{1-M_x^2}\right)^{2\mu}\left(\frac{1-\alpha_{mn}M_x}{1-M_x^2}\right)^{2v}. \tag{17}$$

Under this indexing convention the source distributions of Eq. (17) take the index pairs: (μ,v) for volume acceleration sources, $(\mu,v)=(0,1)$ for volume velocity (monopole) sources$(\mu,v)=(0,2)$, for volume displacement sources, and $(\mu,v)=(0,1)$ for axial dipole sources. For sources of non-zero spatial order, $\mu>0$, the mode amplitudes are non-monotonic functions of the cut-on ratio α, dropping to zero at $\alpha_{mn}=M_x$. This condition occurs at the zero-Mach number cut-off frequency $\omega=c\kappa_{mn}$. Eq. (17) in Eq. (10) gives the following general expression for the non-dimensional ratio of incident sound power and mean square pressure averaged over a duct cross-section:

$$\beta_S^{(\mu,v)}=\frac{\left(1-M_x^2\right)^2\sum_{m,n}\alpha_{mn}^{-1}(1-\alpha_{mn}M_x)^{2(v-1)}(M_x-\alpha_{mn})^{2\mu}}{\sum_{m,n}\alpha_{mn}^{-2}(1-\alpha_{mn}M_x)^{2v}(M_x-\alpha_{mn})^{2\mu}}. \tag{18}$$

4.2. Equal energy per mode and equal energy density per mode

Two alternative source models are the assumption that all cut-on modes carry equal power, and that all cut-on modes produce equal energy density (total acoustic energy per unit volume). Evidence to support the latter as being the most appropriate model for fan noise in ventilation ducts is presented in Ref. [5]. For equal energy per mode we set $\bar{W}_{mn}=\varpi$ in Eq. (9). The resulting mode amplitude distribution $|a_{mn}^{(ee)}|^2$ is

$$\left|a_{mn}^{(ee)}\right|^2=2\rho cS^{-1}\alpha_{mn}^{-1}\varpi\frac{(1-\alpha_{mn}M_x)^2}{(1-M_x^2)}. \tag{19}$$

For the 'equal energy density per mode' source model we note the following generalized definition of the volume-averaged energy density: $\Pi_{mn}=W_{mn}/Sc_{gmn}$, where c_{gmn} denotes the modal axial group velocity defined by $c_{gmn}=\partial\omega/\partial k_x$. Performing the differentiation on Eq. (3a) yields $c_{gmn}/c=(1-M_x^2)\alpha_{mn}/(1-\alpha_{mn}M_x)$. The resulting expression for Π_{mn} is given in Eq. (20a), and the mode amplitude distribution $|a_{mn}^{(ee)}|^2$ obtained by setting $\Pi_{mn}=\Pi$ is given by Eq. (20b),

$$\Pi_{mn}=\frac{|a_{mn}|^2}{2\rho_0c^2}\frac{(1-M_x^2)}{1-\alpha_{mn}M_x}, \tag{20a}$$

$$\left|a_{mn}^{(ee)}\right|^2=\frac{2\Pi\rho_0c^2(1-\alpha_{mn}M_x)}{(1-M_x^2)}. \tag{20b}$$

Comparison of Eqs. (19) and (20b) with Eq. (18) shows that, in general, the source models based on assumptions about constancy of modal energy are not members of the general family of multipole source distributions of Eq. (18) parameterized on (μ,v). The single exception occurs for $M_x=0$. At zero flow speed the 'equal energy per mode' model, the 'equal energy density per mode' model, and both the incoherent uniform-distribution models of monopoles and axial dipoles all collapse to the single source family, $|a_{mn}|^2\propto\alpha_{mn}^{-2(\mu-1)}$. As discussed in Ref. [4], values of the index $\mu=3/2$ and $\mu=2$ correspond, respectively, to equal energy per mode and a uniform distribution of incoherent monopoles. Setting $\mu=1$ corresponds, simultaneously, to a uniform distribution of

incoherent axial dipoles and equal energy density per mode. This is because, even though the modal sound power is proportional to α, and therefore tends to zero as cut-off is approached, the speed with which this diminishing energy is transmitted along the duct also lessens at precisely the same rate, equal to the zero-flow group velocity α. Thus in the absence of flow, an axial dipole distribution is equivalent to the assumption of constant modal energy density.

Using Eqs. (19) and (20b) in Eq. (10) gives the following expressions for β_S for the case of equal energy per mode and equal energy density per mode:

$$\beta_S^{(ee)} = N\left[\sum_{m,n}\frac{(1-\alpha_{mn}M_x)^2}{\alpha_{mn}}\right]^{-1}, \tag{21}$$

$$\beta_S^{(ee)} = \frac{(1-M_x^2)^2\sum_{m,n}\alpha_{mn}(1-\alpha_{mn}M_x)^{-1}}{\sum_{m,n}(1-\alpha_{mn}M_x)}, \tag{22}$$

where $N=N(ka,\ M_x)$ is the total number of propagating modes. Eqs. (18)–(22) are likely to be inaccurate at low frequencies ($ka<0.5$) where the presence of reflections from the open end can no longer be neglected. The present analysis will be restricted to frequencies above this.

5. Computed β_S versus frequency

The eigenvalues for a hard-walled cylindrical duct of radius a, and a rectangular duct of dimensions a and b, are given by

$$\kappa_{mn} = j'_{mn}/a, \quad \kappa_{mn} = \sqrt{(n\pi/a)^2 + (m\pi/b)^2}. \tag{23a, b}$$

Here, j'_{mn} is the nth stationary value of the Bessel function of order m. Eqs. (18), (21) and (22) were used to compute β_S as a function of non-dimensional frequency ka between 1 and 250 in a circular duct. Predictions were obtained for the axial dipole source distribution, the monopole source distribution, and the assumption of equal energy per mode and equal energy density per mode. The results for the representative Mach numbers of $M_x=0$, ±0.2 and ±0.4 are plotted in Figs. 2–5. The predictions are normalized on the plane wave result $\beta_s=(1+M_x)^2$ of Eq. (25).

These results suggest that the frequency variability of β_S for some source distributions is more greatly affected by flow-speed than others. This variability for the four source models plotted in Figs. 2–5 is quantified in Fig. 6. It shows the variance of β_S normalized on its mean value, calculated over the frequency band $20\leqslant ka\leqslant 30$, as a function of Mach number.

The frequency variability in β_S is observed to increase with increasing flow speed in an exhaust duct but diminish with increasing flow speed in a duct inlet. The axial dipole distribution is most sensitive to flow-speed, as clearly shown in Fig. 2. At zero flow speed β_S remains within a narrow range of values over the entire frequency range. Upon the introduction of the small flow speed of $M_x=\pm0.1$, β_S drops close to zero at the cut-off frequencies. The severity of this 'drop out' phenomenon worsens considerably with increasing M_x. For $M_x=\pm0.3$, typical of the flow speeds in turbofan engine inlets and exhausts, fluctuations in β_S are so rapid, particularly at high frequencies where the modal density is very high, its practical application to determine sound power from acoustic pressure measurements is susceptible to large error. The cause of this

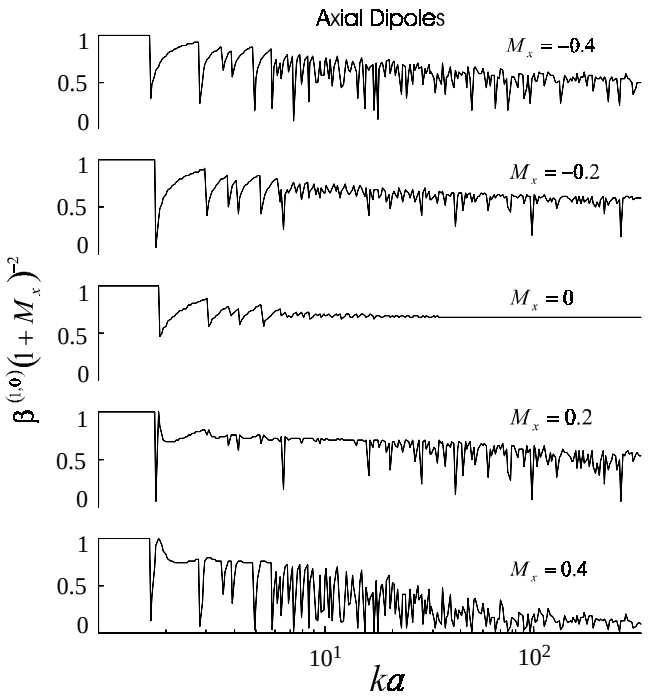

Fig. 2. The ratio β_S of transmitted sound power to mean squared pressure averaged over a duct cross-section evaluated for incoherent *axial dipole* sources uniformly distributed over a duct cross-section for different axial Mach numbers.

behavior is readily explained by the sensitivity of the mode amplitudes to small values of M_x at frequencies very close to cut-off. For $M_x \ll 1$ and $\alpha \ll 1$ in Eq. (18),

$$\frac{\left|a_{mn}^{(\mu,v)}(M_x)\right|^2}{\left|a_{mn}^{(\mu,v)}(0)\right|^2} \approx (1 - M_x/\alpha_{mn})^{2\mu} \quad (M_x \ll 1,\ \alpha_{mn} \ll 1) \tag{24}$$

indicating that for $\mu > 0$ the mode amplitudes at cut-off are finite only for M_x precisely equal to zero. For non-zero Mach numbers the amplitudes of modes close to cut-off tend to infinity leading to the large fluctuations in β_S observed in Fig. 2 for $\mu = 1$. For $\mu = 0$, however, Eq. (24) predicts that the behavior of the mode amplitudes close to cut-off are not affected by flow speed. This is verified in Fig. 3 where fluctuations in β_S are not strongly influenced by M_x. The simulation results of Figs. 2–6 may be summarized as

- The relationship between sound power flow and the mean square pressure in a hard walled, infinite duct generally appears as a highly irregular function of frequency. Frequency irregularity arises from the behavior of individual modes at frequencies close to their cut-off frequencies.
- The frequency irregularity of β_S for sources of non-zero spatial order (e.g., dipoles) is more greatly affected by flow speed than sources of temporal order (e.g., monopole sources). This is due to the sensitivity to flow of the mode amplitudes close to cut-off.

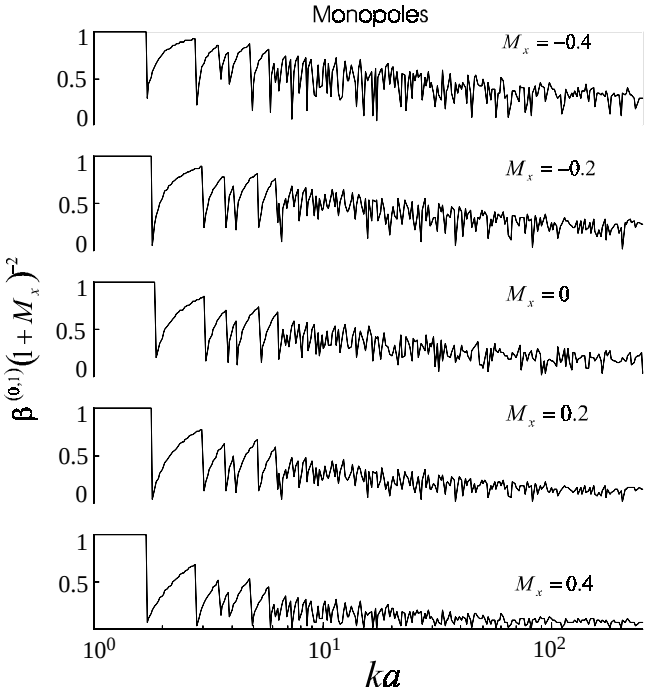

Fig. 3. The ratio β_S of transmitted sound power to mean squared pressure averaged over a duct cross-section evaluated for incoherent *monopole* sources uniformly distributed over a duct cross-section for different axial Mach numbers.

- Frequency irregularity is appreciably less for source models based on constancy of modal energy rather than sources of prescribed multipole order.
- Frequency variability increases with increasing axial Mach number in the duct exhaust, but lessens with increasing Mach number in the duct intake.
- A well-defined high-ka asymptote only exists in some cases. We will show in Section 6 that these are for the source distributions of equal energy per mode, equal energy density per mode at all flow speeds, and for the axial dipole distribution at zero flow speed.

6. Low and high-frequency limiting behaviors of β_S

6.1. Low frequencies: $1 < ka < 1.84$

At the very low frequencies of $ka < 1$, only the plane wave propagates to the open end with significant reflection back along the duct. For duct lengths exceeding one wavelength the in-duct sound field is highly reactive with small sound power–pressure ratio. The sound power estimate at these frequencies is consequently sensitive to measurement error in the acoustic pressure. In the frequency range $1 \leqslant ka \leqslant 1.84/\sqrt{1 - M_x^2}$ plane waves can propagate with negligible reflection from the open end. Setting $N = 1$ and $\alpha = 1$ in Eqs. (18), (21) and (22) gives the source independent plane

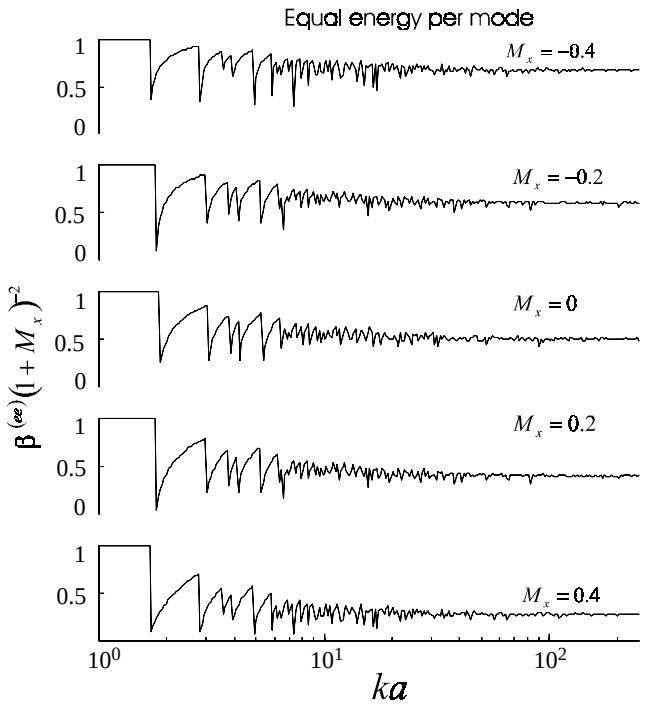

Fig. 4. The ratio β_S of transmitted sound power to mean squared pressure averaged over a duct cross-section evaluated under the assumption of '*equal energy per mode*' for different axial Mach numbers.

wave result

$$\beta_S = (1 + M_x)^2 \quad \left(1 \leqslant ka \leqslant 1.84/\sqrt{1 - M_x^2}\right). \tag{25}$$

6.2. High-frequency limit: $ka \to \infty$

At suitably high ka, the discrete summation of modes in Eq. (10) may be approximated by the integration over a continuum of modes,

$$\beta_S = (1 - M_x^2)^2 \frac{\int_0^1 \left[|a(\alpha)|^2 \alpha n(\alpha)/(1 - \alpha M_x)^2\right] \mathrm{d}\alpha}{\int_0^1 |a(\alpha)|^2 n(\alpha) \mathrm{d}\alpha} \quad (ka \to \infty). \tag{26}$$

Here $n(\alpha)$ is the normalized modal density function defined by

$$n(\alpha) = \left.\frac{N(\alpha + \delta\alpha) - N(\alpha)}{N\delta\alpha}\right|_{\lim \delta\alpha \to 0}, \quad \int_0^1 n(\alpha)\, \mathrm{d}\alpha = 1, \tag{27}$$

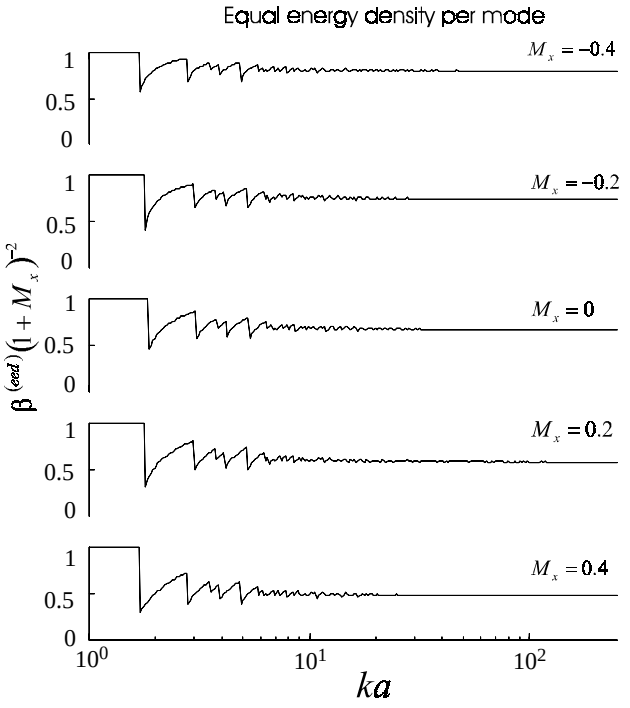

Fig. 5. The ratio β_S of transmitted sound power to mean squared pressure averaged over a duct cross-section evaluated under the assumption of '*equal energy density per mode*' for different axial Mach numbers.

where $N(\alpha)$ is the number of modes with 'α' values of between 0 and α. Following Rice [6], the high-ka asymptotic density function n, expressed in terms of α, is given by

$$n(\alpha) = 2\alpha. \tag{28}$$

Eq. (28) indicates a scarcity of modes that are just cut on compared with a higher population of modes that are well cut on. Eq. (28) in Eq. (26) evaluated for the mode amplitude distribution functions of Eqs. (19) and (20b) give

$$\beta_S^{(ee)} = \tfrac{1}{2}\left(1 - M_x + \tfrac{1}{3}M_x^2\right)^{-1} \quad (ka \to \infty), \tag{29}$$

$$\beta_S^{(eed)} = \frac{6\left(1 - M_x^2\right)\left[\tfrac{1}{2}M_x^{-1} + M_x^{-2} + M_x^{-3}\ln(1 - M_x)\right]}{2M_x - 3} \quad (ka \to \infty). \tag{30}$$

Eqs. (29) and (30) are plotted in Fig. 7.

As both source models are based on assumptions of constancy of modal energy, the two curves follow roughly the same behavior over most of the Mach number range. Evaluating Eqs. (29) and (30) for $M_x = 0$ gives

$$\beta^{(ee)} = \tfrac{1}{2}, \quad \beta^{(eed)} = \tfrac{2}{3} \quad (M_x = 0, ka \to \infty). \tag{31a, b}$$

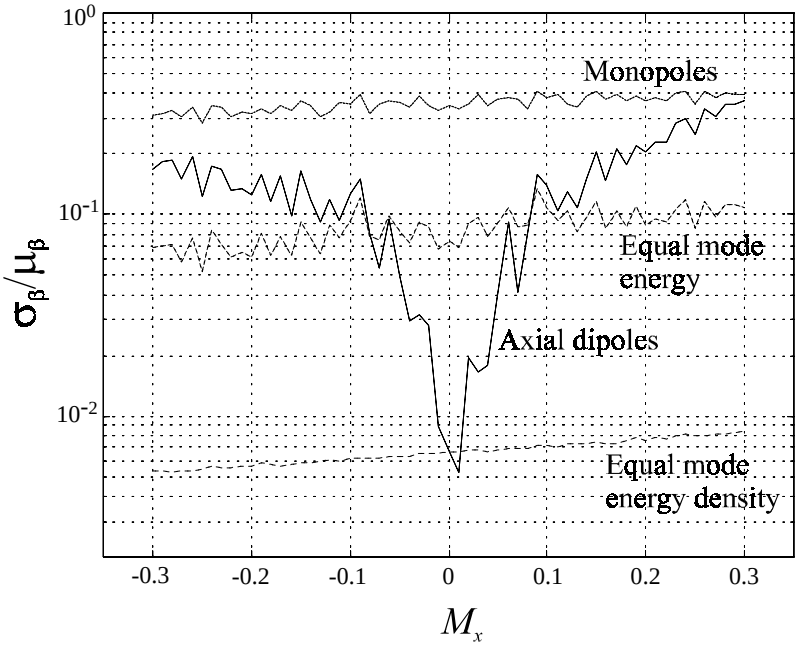

Fig. 6. Normalized variance of β_S calculated over the frequency bandwidth $20 \leqslant ka \leqslant 30$, for four source distributions as a function of axial Mach number.

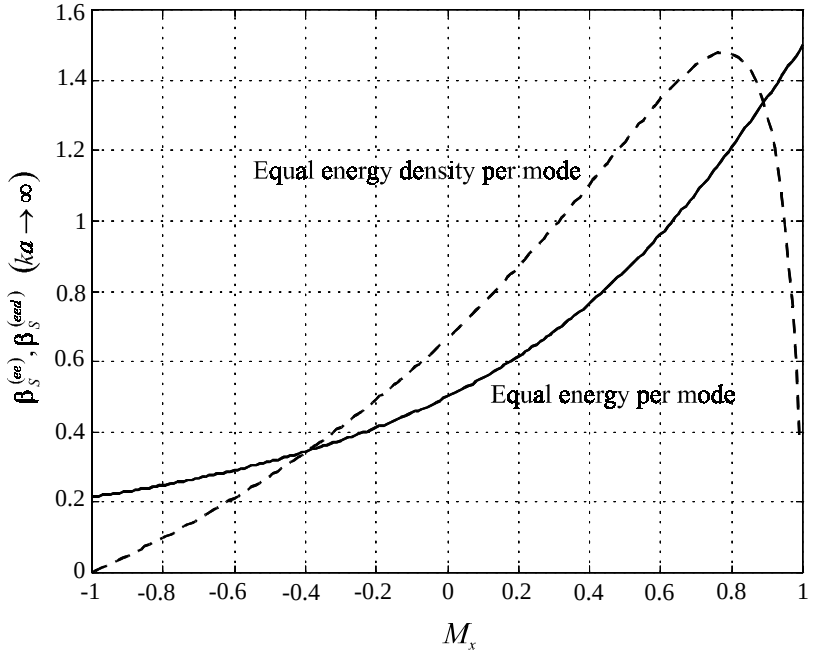

Fig. 7. High-*ka* asymptotic variation of β_S with Mach number for the source models of equal energy per mode, and equal energy density per mode.

Eq. (31a) indicates that, for zero flow, the equal power per mode assumption is equivalent to a hemi-diffuse field in which acoustic energy arrives at the open end from all solid angles equally. Eq. (31b) is identical to that predicted for the axial dipole distribution in zero-flow (Fig. 2) but differs when flow is introduced. As discussed previously in Section 4.2 the axial dipole and equal energy density per mode model are equivalent source models at zero flow-speed.

The corresponding high-ka expression of Eq. (18) for the multipole source distributions, however, generally fails to converge for most (μ,v) combinations. Whilst the numerator of Eq. (18) always converges, and hence the multi-mode transmitted sound power remains theoretically finite, the denominator, which is proportional to mean square pressure, does not. This function diverges slowly to infinity as

$$\lim_{\varepsilon\to 0}\int_{\varepsilon}^{1} 2\alpha^{-1}(1-\alpha M_x)^{2v}(M_x-\alpha)^{2\mu}\mathrm{d}\alpha \to -2M_x^{2\mu}\lim_{\varepsilon\to 0}[\ln\varepsilon]. \tag{32}$$

Eq. (32) explains the tendency observed in Figs. 2 and 3, for β_S to approach zero with increasing ka, to the behavior of modes close to cut-off. The slow logarithmic divergence of this integral indicates that any dissipation present in the duct, for which near-cut-off modes are most affected, will ensure its convergence. The range of parameters in Eq. (32) for which convergence is obtained without dissipation are $\mu>0$ and $M_x=0$, for any value of v. Allowing the Mach number to go to zero offsets the logarithmic growth in ε. For example, putting $v=0$ and $M_x=0$ in Eq. (26) for the amplitude distribution of Eq. (18) gives

$$\beta_S^{(0,\mu)} = \frac{2\mu}{(2\mu+1)} \quad (M_x=0, v=0, ka\to\infty). \tag{33}$$

Physically important cases of Eq. (33) are axial dipoles, $\beta_S^{(0,1)}=2/3$, and axial quadrupoles, $\beta_S^{(0,2)}=4/5$.

6.3. Sound power variation with Mach number

For sources that are not aerodynamic in origin, in the sense that their source strengths are not dependent upon the existence of a flow[2], the present approach may be used to obtain closed form expressions for the high-ka asymptotic sound power variation with M_x. These results are also useful, not only as a means of comparing the β_S-sensitivity of the various source distributions to flow, but also for allowing free-field sound power calculations involving aerodynamic sources to be corrected to include duct convection effects. Writing the high-ka behavior of the mode amplitudes as continuous functions of α and M_x, and using $\chi(ka,\ M_x)$ to denote $N(ka,\ M_x)/N(ka,\ 0)$, the relative increase in the number of modes due to the mean flow, expressions for the high-frequency Mach number variation of the transmitted sound power, compared to its value at $M_x=0$, may be deduced of the form

$$\frac{\bar{W}_x^{(\mu,v)}(M_x)}{\bar{W}_x^{(\mu,v)}(0)} = \chi(ka,M_x)\frac{\int_0^1(1-\alpha M_x)^{2(v-1)}(M_x-\alpha)^{2\mu}\mathrm{d}\alpha}{(1-M_x^2)^{2(\mu+v)}\int_0^1\alpha^{2\mu}\mathrm{d}\alpha} \quad (ka\to\infty), \tag{34}$$

[2] Fan noise is a common example of an aerodynamic source. The Mach number dependence of the transmitted sound power for these sources, particularly at low flow speeds, is dominated by its influence on the source strength. By comparison, the convection effects discussed here, which are a result of modal propagation, are generally much weaker.

$$\frac{\bar{W}_x^{(ee)}(M_x)}{\bar{W}_x^{(\mu,\nu)}(0)} = \chi(ka, M_x) \quad (ka \to \infty), \tag{35}$$

$$\frac{\bar{W}^{(eed)}(M_x)}{\bar{W}^{(eed)}(0)} = \chi(ka, M_x)\frac{\int_0^1 \left[\alpha^2(1-M_x^2)/(1-\alpha M_x)\right] \mathrm{d}\alpha}{\int_0^1 \alpha^2 \mathrm{d}\alpha} \quad (ka \to \infty), \tag{36}$$

In the high-frequency limit ($ka \to \infty$), the ratio $\chi(ka, M_x)$ tends to $(1-M_x^2)^{-1}$. This result follows from Eq. (3b) where the effect of a mean flow is to reduce the cut-off frequencies by the reciprocal of this factor. No general closed-form solution exists to Eq. (34) that is valid for all (ν, μ). However, solutions for the six main source distributions of interest here are given by

$$\frac{\bar{W}_x^{(\,)}(M_x)}{\bar{W}_x^{(\,)}(0)} = \begin{cases} 3M_x^{-3}\left(1-M_x^2\right)^{-1}\left[M_x^4 - M_x^3 - M_x^2 \right. & \\ \quad \left. +2M_x - 2\left(1-M_x^2\right)\ln(1+M_x)\right] & (\mu,\nu) = (1,0), \\ 1 + M_x & (\mu,\nu) = (0,0), \\ \left(1-M_x^2\right)^{-1} & (\mu,\nu) = (0,1), \\ \left(1-M_x^2\right)^{-3}(1 - M_x + \frac{1}{3}M_x^2) & (\mu,\nu) = (0,2), \\ \left(1-M_x^2\right)^{-1} & \text{equal energy per mode}, \\ -3\left(\frac{1}{2}M_x^{-1} + M_x^{-2} + M_x^{-3}\ln(1-M_x)\right) & \text{equal energy density per mode}. \end{cases} \tag{37}$$

Eqs. (37) are plotted in Fig. 8

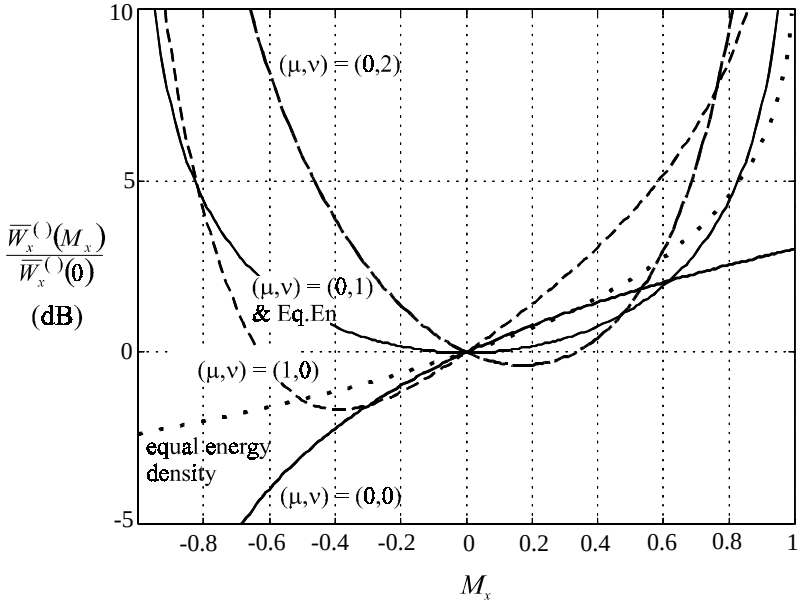

Fig. 8. Multimode, high-ka Mach number dependence of the sound power flow for the source distributions of equal energy per mode, equal energy density per mode, an incoherent distribution of volume displacement sources, volume velocity sources, volume acceleration sources and axial dipole sources uniformly distributed over a duct cross-section.

Generally, the power is predicted to increase with increasing Mach number in the duct exhaust, but decrease with increasing Mach number in the duct inlet. Exceptions are volume displacement sources that have a minimum value of -0.05 dB at $M_x = +0.2$, and axial dipole sources whose minimum value is about -2 dB at $M_x = -0.39$. Other interesting findings are that the equal energy per mode and the volume acceleration source models are predicted to have identical high-ka Mach number dependence. Furthermore, this dependence is an even function of M_x suggesting that their sound power outputs are transmitted upstream and downstream equally.

7. Ratio of sound power to mean squared pressure evaluated at the duct wall

In practice acoustic pressure measurement positions made in a duct carrying a flow are often limited to the wall where the flow speed is much less than in the free stream. Correspondingly, we define a non-dimensional quantity β_a that relates the sound power transmitted along the duct to a single value of the mean square pressure $\overline{p^2}(\mathbf{y}_w)$ at the duct wall,

$$\bar{W} = \beta_a \frac{S\overline{p^2}(\mathbf{y}_w)}{\rho c}. \tag{38}$$

An accurate analysis of this function should include mode shape functions consistent with the shear profile in the real duct, with particular attention being paid to its behavior in the vicinity of the duct wall boundary layer. However, this detailed study is beyond the scope of the current paper and will be investigated in a subsequent report. By restricting the computations to the low flow speeds for which boundary layer effects are negligible β_a may be predicted by combining Eqs. (7) and (8) evaluated at the duct wall. Rather than compute β_a directly, however, we focus on the ratio $\overline{p^2}(\mathbf{y}_w)/\langle \overline{p^2} \rangle_S$, which we will now show has useful high-ka asymptotic properties that are independent of source distribution and flow-speed. This information, in conjunction with knowledge of β_S, may then be used to compute sound power. For incoherent modal addition this ratio becomes

$$\frac{\beta_S}{\beta_a} = \frac{\overline{p^2}(\mathbf{y}_w)}{\left\langle \overline{p^2} \right\rangle_S} = \frac{\sum_{m,n} |a_{mn}|^2 \Psi_{mn}^2(\mathbf{y}_w)}{\sum_{m,n} |a_{mn}|^2}, \tag{39}$$

where $\mathbf{y}_w$ denotes a position on the duct wall. The factor $\Psi_{mn}^2(\mathbf{y}_w)$ specifies the ratio of the mean square pressure at the duct wall to that averaged over a duct cross-section due to a single mode. It therefore has the interpretation as a measure of the degree to which the modal pressure is concentrated at the wall. For rigid circular and rectangular ducts $\Psi_{mn}^2(\mathbf{y}_w)$ is given by

$$\Psi_{mn}^2(\mathbf{y}_w) = \left[1 - (m/\kappa_m a)^2\right]^{-1}, \tag{40}$$

$$\Psi_{mn}^2(\mathbf{y}_w) = \varepsilon_n \varepsilon_m \begin{cases} \cos^2(n\pi y/a), & z = b, \\ \cos^2(m\pi z/b), & y = a, \\ 1, & z = b \text{ and } y = a. \end{cases} \tag{41}$$

Here, $\varepsilon_m = 2$ and 1 for $m \neq 0$ and $m = 0$, respectively. Noting that $\Psi_{mn}^2(\mathbf{y}_w) \geqq 1$ (which for the circular ducts following the Bessel function property, $m < j'_{mn}$) suggests that $\overline{p^2}(\mathbf{y}_w) \geqslant \langle \overline{p^2} \rangle_S$. By

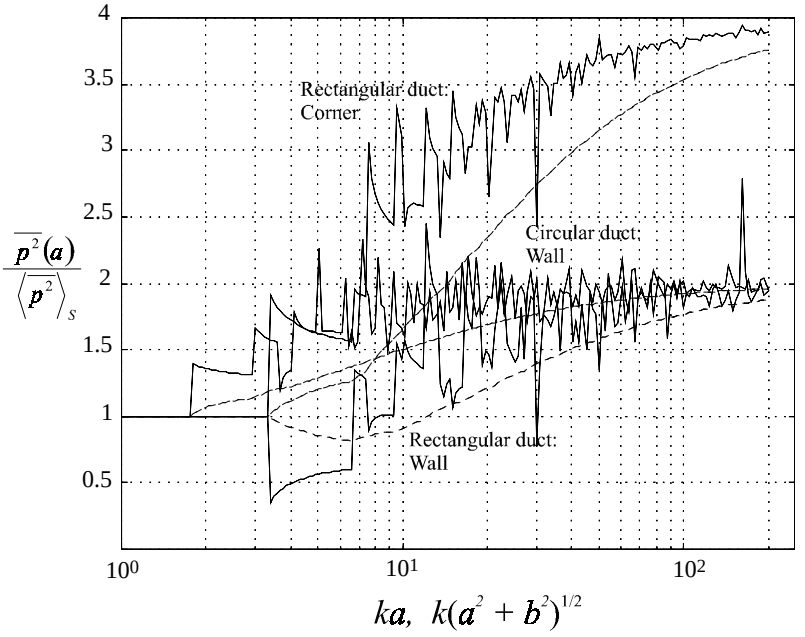

Fig. 9. Mean square pressure at the wall divided by that average over a duct cross-section evaluated for the case of equal energy per mode with $M_x = 0.3$. Examples shown for a rectangular duct in the corner, rectangular duct on the wall but away from the corner, and on the wall of a circular duct. Smooth curve denotes $\mathrm{E}\{\Psi^2_{\mathrm{mn}}(\mathbf{y}_{wall})\}$.

way of example, Eq. (39) was computed for the case of equal energy per mode, $M_x = 0.3$, in the corner and on the wall (but well away from corner) of a rectangular duct with dimensions of $a = 0.4$, $b = 0.92$ ($a^2 + b^2 = 1$), and on the wall of a circular duct. The smooth curves in Fig. 9 represent the mean of $\Psi^2_{mn}(\mathbf{y}_w)$ for the three cases.

For practical purposes, the important aspect of these results is their high-frequency asymptotes. These are predicted to be 4 in the case of the rectangular duct for the corner measurement, and 2 for measurements made at the wall of both rectangular and circular ducts. These asymptotes are found to be independent of either source distribution or Mach number. The smooth curves in these figures, which have the correct high-ka limiting behavior, represents a statistical lower-bound for the local mean of $\overline{p^2}(\mathbf{y}_w)/\langle \overline{p^2} \rangle_S$. It is obtained by treating $|a_{mn}|^2$ and $\Psi^2_{mn}(\mathbf{y}_w)$ in Eq. (38) as independent random variables and regarding the modal summation $\sum_{m,n}$ as an expectation $E\{\ \}$. Under these assumptions, Eq. (39) becomes $\overline{p^2}(\mathbf{y}_w)/\langle \overline{p^2} \rangle_S = \mathrm{E}\{\Psi^2_{mn}(\mathbf{y}_w)\}$. However, for the source distributions under consideration the function $\Psi^2_{mn}(\mathbf{y}_w)$ is observed to consistently underestimate the ratio of mean square pressures. Thus

$$\frac{\overline{p^2}(\mathbf{y}_w)}{\left\langle \overline{p^2} \right\rangle_S} = \frac{\mathrm{E}\{|a_{mn}|^2 \Psi^2_{mn}(\mathbf{y}_w)\}}{\mathrm{E}\{|a_{mn}|^2\}} \geqslant \mathrm{E}\{\Psi^2_{mn}(\mathbf{y}_w)\}. \tag{42}$$

This finding suggests that, rather than being independent parameters, $|a_{mn}|^2$and $\Psi^2_{mn}(\mathbf{y}_w)$ are correlated from which one can infer that the covariance between the two factors is positive. Thus,

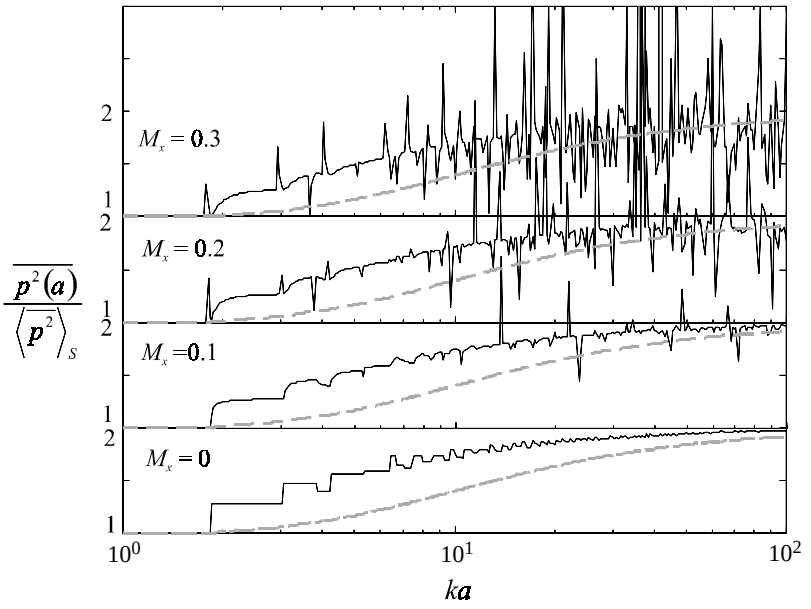

Fig. 10. Ratio of mean squared pressure at the duct wall to that averaged over a duct cross-section for a uniform distribution of *axial dipole* sources distributed over a duct cross-section. Smooth curve denotes $\mathrm{E}\{\Psi^2_{\mathrm{mn}}(a,\theta)\}$.

there is a tendency for modes of large amplitude to have their pressure distributions concentrated at the duct wall. This is certainly true in circular ducts for the modes with large m value near cut-off, for which $j'_{mn} \approx m$. In this case both the mode amplitude and modal factor $\Psi^2_{mn}(\mathbf{y}_w)$ are comparatively large as predicted by Eqs. (17) and (40), respectively. The usefulness of Eq. (43) is that its right-hand side is independent of mode amplitude distribution and, for ka greater than about 10, it incurs less than 20% error (≈ 1 dB) for the source distributions under investigation. Furthermore, it has the correct low-ka and high-ka asymptotes of $\mathrm{E}\{\Psi^2_{mn}(\mathbf{y}_w)\} \to 1$ and $\mathrm{E}\{\Psi^2_{mn}(\mathbf{y}_w)\} \to 2$, respectively.

We now explore the variation of $\overline{p^2}(\mathbf{y}_w)/\langle \overline{p^2} \rangle_S$ with source distribution and Mach number for a circular duct with $\mathbf{y}_w = (a, \theta)$. Figs. 10–12 depicts its behavior for the axial dipole, monopole and equal energy per mode distributions for a range of flow Mach numbers.

These figures indicate that, whilst the general behavior is roughly the same, including the same asymptote, differing source distributions and Mach numbers significantly affect the variability of the relationship between pressure measurements made at the wall and that averaged over a duct cross-section. It remains to be shown whether frequency averaging, or the introduction of dissipative liners, will significantly smooth this variability to a degree that permits its application to measured data.

8. Experimental verification

8.1. Experimental set-up

Preliminary measurements have been made aimed at verifying experimentally some of the main no-flow results presented in this paper. Measurements were made without flow in a circular duct

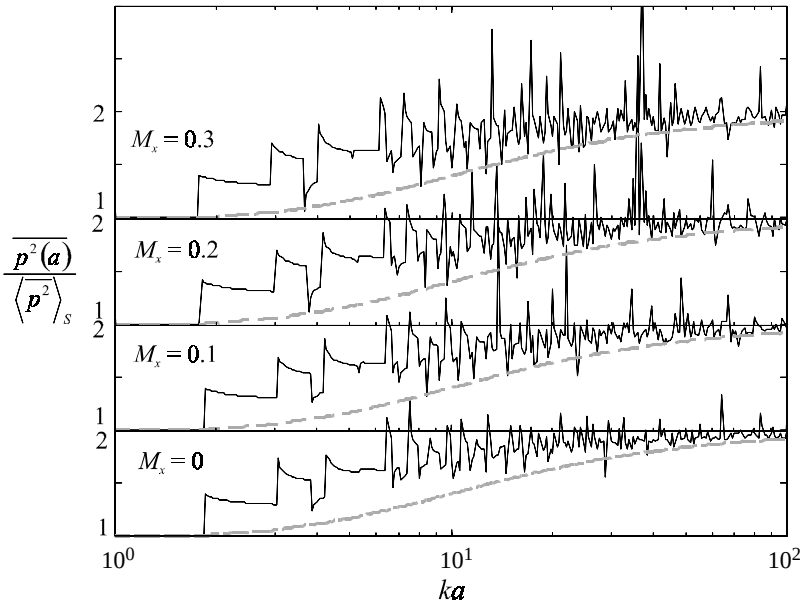

Fig. 11. Ratio of mean squared pressure at the duct wall to that averaged over a duct cross-section for the source mode, *equal energy per mode*. Smooth curve denotes $\mathrm{E}\{\Psi^2_{\mathrm{mn}}(a,\theta)\}$.

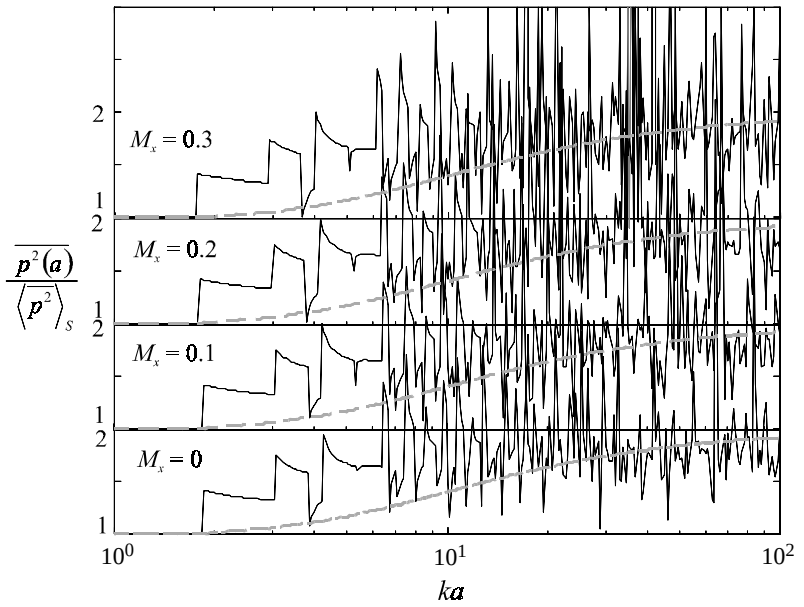

Fig. 12. Ratio of mean squared pressure at the duct wall to that averaged over a duct cross-section for a uniform distribution of monopole sources distributed over a duct cross-section. Smooth curve denotes $\mathrm{E}\{\Psi^2_{\mathrm{mn}}(a,\theta)\}$.

of (i) the ratio between the radiated sound power to the mean square pressure averaged over the duct cross-section, and (ii) the ratio between the mean square pressure at the duct wall to that averaged over a duct cross-section. The duct used was a rigid plastic tube of length 1 m, with

Fig. 13. Photograph of duct taken from receiver room looking into the duct.

0.23 m internal diameter, and a wall thickness of 10 mm. It was located midway though the joining wall of two reverberation rooms, both of 13.1 m^3 in volume. One reverberation chamber, excited by a loudspeaker driven by random broadband noise, was used to provide the diffuse field excitation of the in-duct sound field necessary to create the condition of 'equal energy per mode' in the duct.[3] The other reverberation chamber was used to determine the steady state radiated sound power using the Sabine energy balance technique. Photographs looking into the duct from the receiver room are presented in Fig. 13.

The sound field within the duct was measured by a small electret microphone attached to a thin rod (shown above) that was allowed to slide between two small diametrically opposite holes. The measurement plane was located approximately 30 cm from the end of the duct to reduce the influence of reflected cut-off modes. This mechanism allowed the traverse of the microphone along a duct diameter, which were undertaken in 11 equal increments. Precautions were taken to ensure that the microphones were positioned close to, but not touching, the walls. At each radial position the acoustic pressure was measured circumferentially at every 60° by rotating the duct about its axis. A microphone positioned in the receiver room was used to determine the radiated sound power from the average of the mean square pressure obtained at seven different positions around the room. Each pressure measurement made in the duct and in the receiver room was then averaged over six loudspeaker positions in the source room to increase the 'diffuseness' of the excitation sound field.

Spectral acoustic measurements made inside the duct and in the receiver room were derived from 200, 2048 point FFT averages at a sampling frequency of 51.2 kHz. This corresponds to a 25 Hz resolution over a 25 kHz bandwidth. The receiver room reverberation time was measured in third-octave bands to give a Schröder frequency of 766 Hz, corresponding to $ka = 1.7$ in duct-frequency units. This data was also used to determine the Sabine absorbing area as a function of frequency for subsequent sound power determination.

The measured ratio between the pressure spectrum and that averaged over the duct cross-section obtained using a discrete approximation to $\langle \overline{p^2} \rangle_S$ is presented below (solid curve) in Fig. 14. Also shown (dashed curve) is the theoretical prediction, obtained assuming equal energy

[3] The equivalence between the assumption of 'equal energy per mode' and the hemi-diffuse field was demonstrated in Eq. (31a). The converse is true by reciprocity.

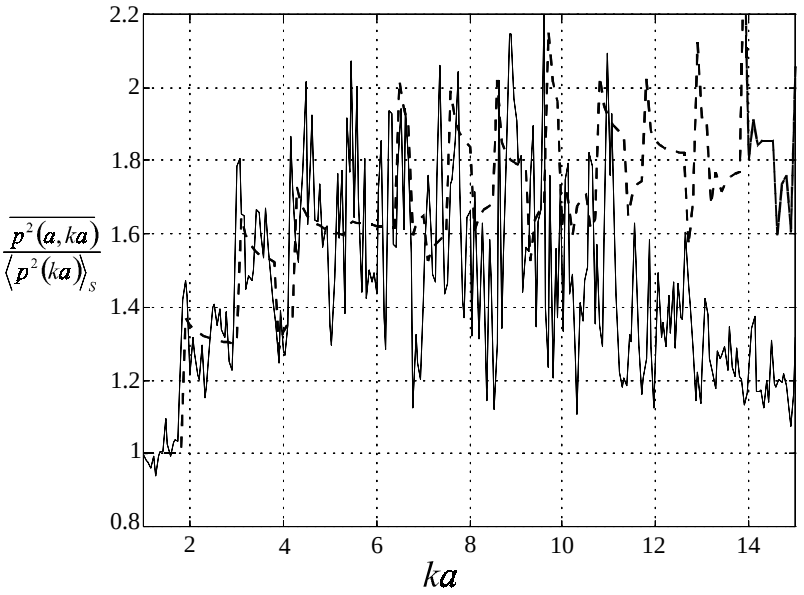

Fig. 14. Ratio of pressure spectrum at the wall of a hard-walled duct to its value averaged over a duct cross-sectional area. Comparison between measured result (dashed curve) and theoretical prediction (solid curve).

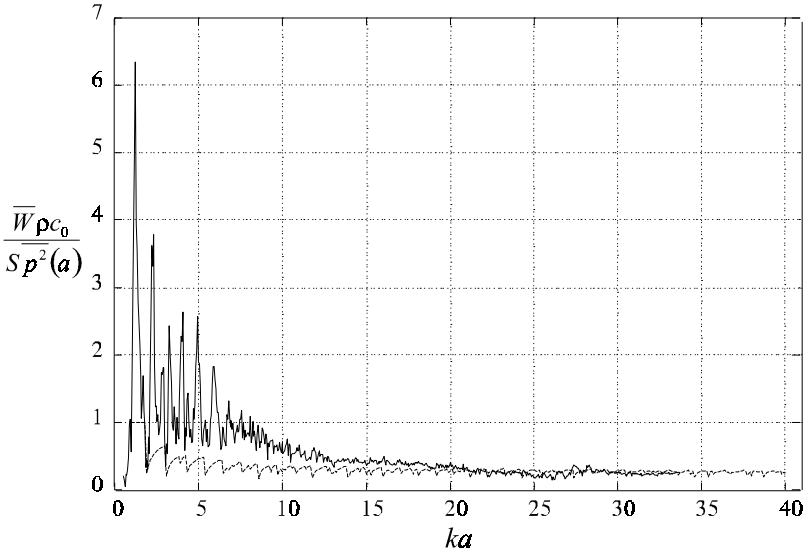

Fig. 15. Comparison between measured value of the quantity β_S, defined by Eq. (4) under diffuse field excitation, and that predicted by Eq. (22) for $M_x = 0$.

per mode. For consistency, the same discrete approximation to the surface-averaged mean square pressure used in the measurements was used in the prediction.

Agreement between the experimental and theoretical curves is excellent at *ka* less than about 10 (about 5 kHz). Much of the fine detail present in the predictions, including the sharp

discontinuities at the cut-off frequencies, is faithfully reproduced in the measurements. Oscillations present in the experimental results, but not in the predictions, can be attributed to axial standing waves that are not included in the infinite-duct model. At ka exceeding 10 the experimental results begin to fall below the predicted values. Duct-wall vibrations are unlikely to be the cause of this discrepancy. Accelerometer measurements made at the duct wall reveal that wall vibrations are greatest at ka less than about 4, and drop by 30 dB at frequencies above this. Explanations for these differences at high frequencies are currently being sought.

Fig. 15 presents a comparison between the measured variation of β_a versus frequency (solid curve) and the predicted variation obtained from the prediction in Fig. 4 of $W\rho c/S\langle\overline{p^2}\rangle$ divided by the prediction in Fig. 11 of $\overline{p^2}(a)/\langle\overline{p^2}\rangle_S$ for $M_x=0$.

Contrary to the results in Fig. 14, extremely good agreement between the measured and predicted curves is observed at ka exceeding 10, and very poor match is observed below it. The most likely explanation of this low-frequency discrepancy is the presence of axial standing waves in the duct. Modal reflection is known to be most significant at the cut-off frequency in which the modes strike the open end at angles close to 90° to the duct axis. However, reflected modes will not affect the results presented in Fig. 11, which were measured in the same plane.

9. Conclusions

A non-dimensional parameter β_S has been derived and computed that relates the total sound power propagating towards the open end of a duct containing a uniform flow to measurements of the mean-squared pressure averaged over a duct cross-section, and to a single-pressure measurement made at the duct wall. Expressions are presented to allow the computation of this relationship for an incoherent distribution of sources of arbitrary temporal and spatial order uniformly distributed over a duct cross-section. Also investigated are the source models of 'equal energy per mode' and 'equal energy density per mode'. Calculations shows that

- The relationship between sound power flow and the mean square pressure in a hard walled, infinite duct is generally a poorly behaved, highly oscillatory function of frequency.
- Frequency variability is highest for source distributions of temporal, rather than spatial, order
- Frequency variability increases with increasing axial Mach number, but is less in the duct intake than in the duct exhaust.
- Frequency irregularity is appreciably less for source models based on constancy of modal energy rather than of multipole order.
- A well-defined high-ka asymptote is only observed in some cases. These are for the source distributions of equal energy per mode and for the axial dipole distribution at zero Mach number.
- The mean square pressure at the duct wall bears a simple relationship to its mean square value averaged over the duct cross-section, that is only weakly dependent upon the mode amplitude distribution. In the high-ka limit, the ratio between the two measurements tends to two.

Preliminary measurements of the radiated sound power and in-duct pressure made in the absence of flow are used to determine β_S and $\overline{p^2}(a)/\langle\overline{p^2}\rangle$ experimentally. The duct was

terminated into a reverberation chamber for the purpose of exciting the ducted sound field by a high-frequency reverberant sound field in order to approximate to the condition of equal energy per mode. Close agreement with theoretically predicted values of β_S is obtained for ka values less than 10, but not at frequencies above. The reason for this discrepancy has so far not been satisfactorily resolved.

References

[1] D.H. Munroe, K.U. Ingard, On acoustic intensity measurements in the presence of mean flow, Journal of the Acoustical Society of America. 65 (1979) 1402–1406.
[2] W. Neise, F. Arnold, On sound power determination in flow ducts, Journal of Sound and Vibration 244 (3) (2001) 481–503.
[3] C.L. Morfey, Sound transmission and generation in ducts with flow, Journal of Sound and Vibration 14 (1971) 37–55.
[4] P. Joseph, C.L. Morfey, Multi-mode radiation from an unflanged, semi-infinite circular duct, Journal of the Acoustical Society of America 105 (5) (1999) 2590–2600.
[5] W. Frommhold, F.P. Mechel, Rechnerische Untersuchungen zur Bestimmung der Schalleistung in Rechteckkanaklen Fraunhofer-Institut für Bauphysik, BS 202/89 (1989).
[6] E.J. Rice, Multimodal far-field acoustic radiation pattern using mode cutoff ratio, American Institute of Aeronautics and Astronautics Journal 16 (1978) 906–991.